

Charge-resonance-enhanced ionization of molecular ions in intense laser pulses: Geometric and orientation effects

André D. Bandrauk and Jonathan Ruel

Laboratoire de Chimie Théorique, Faculté des Sciences, Université de Sherbrooke, Sherbrooke (Québec), Canada J1K 2R1

(Received 4 September 1998)

Numerical solutions of the time-dependent Schrödinger equation for one-electron two-dimensional H_2^+ , H_3^{2+} molecular ions have been obtained in order to illustrate the dependence of charge-resonance-enhanced ionization (CREI) on the angular orientation of the molecule. For H_3^{2+} both linear and triangular geometries have been considered. It is found, in general, that orientational effects on ionization rates, laser-induced dipole moments and torques, are most significant at the critical distances R_c and critical angles ϕ_c of molecular geometry where CREI occurs. The calculated ionization rates and field-induced torques are used to estimate alignment times near the dissociative ionization regime of these ions in intense laser pulses. It is found that orientational trapping can occur in this regime at the critical CREI configurations. [S1050-2947(99)06303-9]

PACS number(s): 42.50.Hz

I. INTRODUCTION

The behavior and properties of atoms and molecules in intense laser fields is an area of research exploring the nonlinear, nonperturbative response of these systems in the presence of intense short laser pulses. In the case of atoms, considerable progress and understanding of phenomena such as above threshold ionization, high-frequency stabilization, and high-order harmonic generation has been recently summarized by Gavrilá [1]. Similar nonlinear, nonperturbative effects have now been found in molecules [2], where an extra degree of freedom, the internuclear motion, leads to some effects such as above threshold dissociation vibrational trapping due to laser-induced avoided crossings, [2] and most recently charge-resonance-enhanced ionization (CREI) [3–5]. In the latter molecular ion ionization rates are enhanced by one or two orders of magnitude at critical internuclear distances R_c with respect to the fragments of the corresponding molecule. Calculations [3–6] and measurements of CREI on linear molecules [7–9] have usually assumed that the molecular ion is aligned with the field. Recent Coulomb explosion experiments show considerable spread of angular distribution of the fragments [7,10–12], thus raising the question of alignment or orientation time in dissociative ionization experiments as compared to recent nondissociative, nonionization estimates [13,14].

In the present work we present exact numerical solutions of the time-dependent Schrödinger equation (TDSE), for two-dimensional models of two one-electron molecular ions, H_2^+ and H_3^{2+} . In both cases, CREI has been found previously to occur at critical internuclear distances $R_c = 4/I_p \approx 8$ a.u. [4] for H_2^+ and $R_c = 5/2I_p \approx 5$ a.u. for linear H_3^{2+} [6]. Both critical distances have been analytically derived from a laser-induced static barrier suppression model for molecular ionization originally suggested by Codling *et al.* [15]. We have shown in [3–6] that inclusion of the charge-resonance coupling of the doorway states, $1\sigma_g$ and $1\sigma_u$ orbitals for H_2^+ , $2\sigma_g$, $1\sigma_u$, and $1\sigma_g$ for H_3^{2+} , as discussed earlier by Mulliken [16] for molecular absorption spectroscopy, is essential to reproduce the critical distances R_c at

which enhanced ionization occurs. Numerical simulations with fixed nuclei [3–6,17] and full dynamical non Born-Oppenheimer calculations [18,19], and experiments [8,9,14] confirm the model of over-barrier ionization of the molecular electrons via the CREI mechanism in the presence of intense laser pulses. Recent work on ionization of large polyatomic molecules by intense laser pulses further suggests that a static field ionization mechanism is also operative [20,21].

The present work examines the orientation dependence of the ionization rates in quantum-mechanical two-dimensional (2D) numerical solutions of the TDSE for fixed nuclear configurations of H_2^+ and both linear and triangular H_3^{2+} . The exact numerical solutions of the electronic wave function for fixed nuclei and angle allow also for calculating the time-dependent torques experienced by each molecular ion. The numerical results are used to estimate the alignment times of H_2^+ and H_3^{2+} in the dissociative-ionization regime of these molecules in the presence of a laser of wavelength 1064 nm around intensities $I = 10^{14}$ W/cm².

II. NUMERICAL METHOD FOR THE TDSE

The one-electron TDSE for both one-electron molecular ions H_2^+ and H_3^{2+} is solved in a two-dimensional (x,z), 2D model using Coulomb-modified potentials, used especially in plasma physics in order to avoid singularities in classical numerical integration schemes [22,23]. The laser field is assumed polarized along the x axis so that the z axis corresponds to $\theta = \pi/2$. The general one-electron TDSE for a linearly polarized laser field $E(t) = E_0(t) \cos \omega t$, of frequency ω and pulse envelope $E_0(t)$ with peak intensity E_0 is written in atomic units ($e = \hbar = m_e = 1$) as

$$i \frac{\partial \psi(x,z,R,\theta,t)}{\partial t} = \left[-\frac{1}{2} \nabla_{x,z}^2 + V_c + V_N + xE_x(t) + zE_z(t) \right] \times \psi(x,z,R,\theta,t), \quad (1)$$

where

$$V_c = - \sum_{i=1}^N [(x_i^2 + z_i^2) + c]^{-1/2}, \quad (2)$$

is the softened Coulomb potential ($c=0$ corresponds to the pure Coulomb potential). $N=2$ for H_2^+ and 3 for H_3^{2+} , and x_i, z_i are the electron coordinates with respect to the i th nucleus. V_N is the total nuclear repulsion and the last two terms represent the two components of the field-electron interaction ($x: \theta=0$; $z: \theta=\pi/2$). With $c \neq 0$ in the regularized Coulombs potential, one can solve the total TDSE equation (1) and thus obtain the electronic wave function $\Psi(x, z, R_i, \theta, t)$ for different nuclear configurations R, θ at various times t . Absorbing boundaries are used to remove electron flux from the finite-size 2D grid in x and z thus allowing for calculation of the ionization rates from the norm of the function (we drop the nuclear and field coordinates for convenience)

$$N(t) = \int |\psi(x, z, t)|^2 dx dz = \sum_{i,j=-N/2}^{N/2} |\psi(i, j, t)|^2 (\Delta m)^2, \quad (3)$$

where Δm is the distance between grid points and N the number of grid points in each dimension.

The ionization rate Γ is obtained from the logarithmic decrease of the norm, $\ln N(t) = -\Gamma t$. Time-dependent observables such as the dipole component d_x are calculated from the discretized function as

$$d_x(t) = \langle \psi(x, z, t) | x | \psi(x, z, t) \rangle = \sum_{i,j}^{\pm N/2} \psi^*(i, j, t) x_i \psi(i, j, t) (\Delta m)^2. \quad (4)$$

The minimum grid-point separation for accurate calculations is determined by the uncertainty principle $\Delta x \Delta p \approx 1$. Thus, since electrons are expected to acquire energies up to 20 Up, in molecules [24] where $\text{Up} = E_0^2/4\omega^2$ is the ponderomotive energy, we set the maximum $\Delta p = (2E)^{1/2} = (40 \text{ Up})^{1/2}$ which determines the minimum Δx . Similarly the minimum Δt is set below $\pi/(3\Delta E) = \pi/(60 \text{ Up})$ in the time integration when one uses fast Fourier transform methods for the kinetic energy [25]. Due to the avoidance of singularities with the regularized Coulomb potential (2), we use a split-operator method of accuracy $(\Delta t)^3$. The numerical accuracy is verified by using at different time intervals higher-order accuracy schemes [26]. In the present calculation at intensities $I_0 = cE_0^2/8\pi = 8 \times 10^{13} \text{ W/cm}^2$ (4.8×10^{-2} a.u.) and $\lambda = 1064 \text{ nm}$ ($\omega = 5.3 \times 10^{-2}$ a.u.), then $\text{Up} = 0.39 \text{ a.u.} \approx 11 \text{ eV}$. We have used therefore $\Delta x = 0.25 \text{ a.u.}$, $\Delta t = 0.03 \text{ a.u.}$ with a pulse length of 30 cycles which is ramped to the maximum E_0 in 5 cycles.

The c value for the regularized Coulomb potentials (2) was set at $c=0.5$. In the present 2D calculations, we found this value of c to give ionization potentials I_p closest to our previous exact 3D calculation for H_2^+ [3,4] and H_3^{2+} [6]. In particular, only with $c=0.5$ can one reproduce the double peak structure of the ionization rate (Γ) as a function of the internuclear distance R first calculated for H_2^+ [3,4]. This double peak structure with maxima at the critical distances

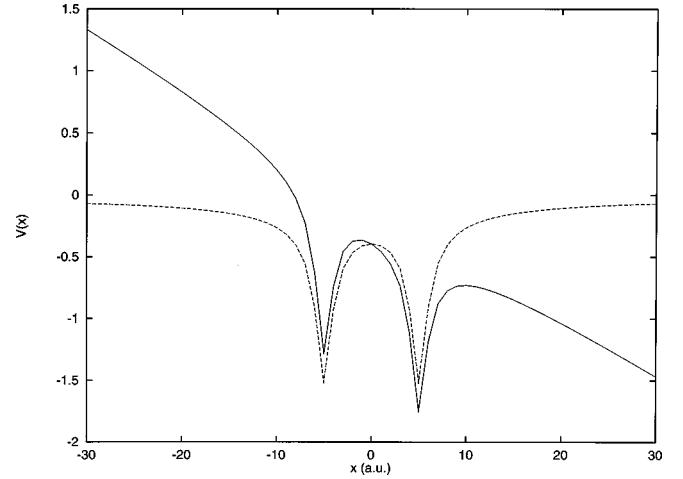


FIG. 1. Electron potential energy $V(x) = V_c + E_0 x$ (solid line) for H_2^+ in a static field $E_0 = 4.8 \times 10^{-2}$ a.u. ($I = 8 \times 10^{13} \text{ W/cm}^2$) parallel to the x (molecular) axis at internuclear distance $R = 10$ a.u. as compared to zero field (dotted line).

$R_c = 7$ and 10 a.u. has now been confirmed experimentally [9]. At the latter critical distance, 10 a.u. for H_2^+ , we find for the 2D model $I_p = 0.636$ a.u. as compared to 0.6 a.u. in the exact 3D case. The corresponding ionization rates are $2 \times 10^{13} \text{ s}^{-1}$ (2D) vs $0.8 \times 10^{13} \text{ s}^{-1}$ (3D).

Since we shall interpret the ionization results in terms of static field plus Coulomb potential barriers (e.g., [4–6,17]), we plot in Figs. 1 and 2 the net electrostatic potentials, which influence the electronic motion in H_2^+ (Fig. 1) for laser field parallel to the internuclear x axis ($\theta=0$) and for equilateral H_3^{2+} (Fig. 2) for the laser field parallel to the z axis ($\theta = \pi/2$). We show both zero field potentials V_c (dotted) and the field-induced potentials $E_0 + V_c$ (solid) at $E_0 = 4.8 \times 10^{-2}$ a.u. ($I_0 = 8 \times 10^{13} \text{ W/cm}^2$) with $c=0.5$ in Figs. 1 and 2. Thus in the case of H_2^+ , the symmetric double well at

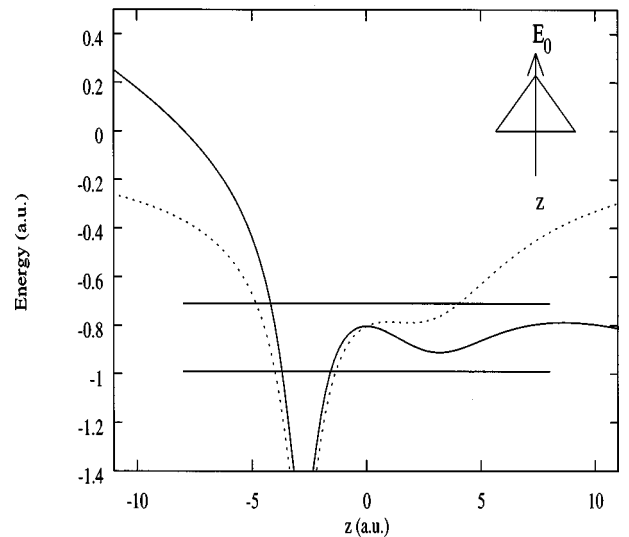


FIG. 2. Electron potential energy $V(z) = V_c + E_0 z$ (solid line) for an equilateral H_3^{2+} ($\phi=60^\circ$) in a static field $E_0 = 4.8 \times 10^{-2}$ a.u. ($I = 8 \times 10^{13} \text{ W/cm}^2$) parallel to the z axis (perpendicular to any bond) at interproton distance $R = 6.5$ a.u. as compared to zero field (dotted line).

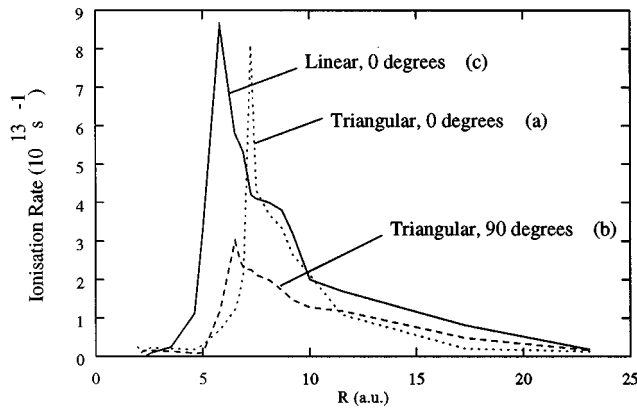


FIG. 3. Ionization rates Γ (10^{13} s^{-1}) in a $\lambda=1064 \text{ nm}$, $I=8 \times 10^{13} \text{ W/cm}^2$ laser field for equilateral H_3^{2+} as a function of interproton distance R (a.u.): (a) equilateral for x polarization; (b) equilateral for z polarization; (c) linear parallel to x polarization.

$E_0=0$ is distorted in the direction of the laser field E_0 allowing for escape of the electron at the peak value E_0 of the field through charge resonance effects [4–6]. In the case of triangular H_3^{2+} , the static-field-induced ionization path, Fig. 2(b), is modified from the pure atomic case (one well at $z < 0$) by an extra minimum due to the presence of the other two nuclei.

III. CREI IN NONLINEAR H_3^{2+}

In the preceding section, we described the numerical methods for obtaining accurate ionization rates, which as shown in Figs. 3 and 4 manifest maxima at critical distances R_c and angles θ_c due to CREI. These large ionization rates in molecular ions exceed that of the dissociation fragments by one or two orders of magnitude in the presence of short intense laser pulses, and were first obtained in numerical simulations and correlated to laser-induced charge localization [3]. Expressions for R_c have been derived for linear H_2^+ and H_3^{2+} based on an electrostatic model wherein the electron is excited to a field-induced lowest unoccupied molecular (LUMO) from a highest occupied molecular orbital (HOMO) and escapes through charge-resonance effect above the internal barriers induced by the static laser field E_0 and the internal Coulomb potential V_c , Eq. (2) (see Figs. 1 and 2). Thus for H_2^+ one obtains $R_c=4/I_p=8 \text{ a.u.}$ [5], whereas for linear H_3^{2+} , $R_c=5/2I_p=5 \text{ a.u.}$ [6], where R is the interproton distance. This theoretical prediction which includes the charge-resonance energy displacement of the LUMO is in excellent agreement with exact 3D [4,6] and 1D [5] simulations. This has been shown to be also independent of field intensity and nuclear charge [5,6]. The charge-resonance effect occurs through the strong coupling between the free field HOMO and the corresponding LUMO by the radiative coupling $\mu(R)E_0$ where $\mu(R)$ is the electronic transition moment between these two “frontier” orbitals [27,28]. For H_2^+ , $\mu(R)=R/2$, whereas for linear H_3^{2+} , $\mu(R)=R/2\sqrt{2}$.

We illustrate in Fig. 3 the ionization rate for triangular, equilateral H_3^{2+} as a function of the interproton distance R for $\lambda=1064 \text{ nm}$, $I=8 \times 10^{13} \text{ W/cm}^2$ laser conditions. Curve (a) corresponds to the electric field polarized along the x axis, i.e., parallel to one of the bonds whereas (b) corre-

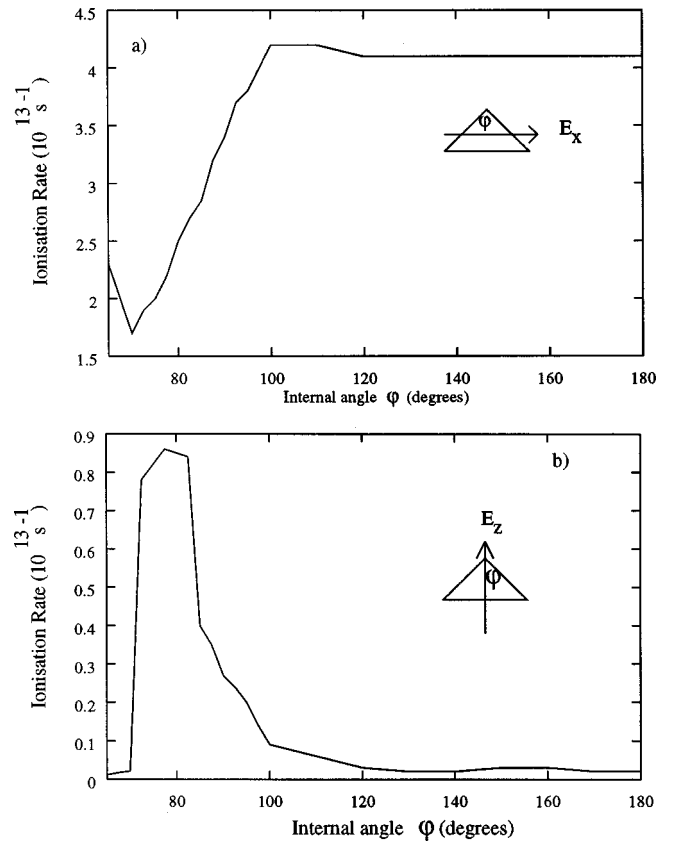


FIG. 4. Ionization rates Γ (10^{13} s^{-1}) as a function of an internal bond angle ϕ for H_3^{2+} in $\lambda=1064 \text{ nm}$, $I=8 \times 10^{13} \text{ W/cm}^2$ laser field; (a) x polarization ($\theta=0$); (b) z polarization ($\theta=\pi/2$).

sponds to z -axis polarization, i.e., perpendicular to one of the bonds. (c) is the corresponding ionization rate curve for the field parallel to a linear H_3^{2+} . One notes that the triangular equilateral configuration (a) behaves very similarly to the linear molecular, curve (c), for parallel bond polarization. The critical distance R_c for CREI is somewhat larger, $R_c \approx 7 \text{ a.u.}$, for the triangular configuration as compared to $R_c \approx 5 \text{ a.u.}$ for the linear configuration. This small difference in R_c 's reflects the difference in energy of the HOMO and LUMO for the linear [(c)] and triangular [(a)] configurations. In the linear case, the two orbitals are separated by a smaller electronic transfer energy β , whereas for the equilateral configuration, the LUMO is doubly degenerate with a larger energy separation from the HOMO [27]. Thus one must go to longer internuclear distances in the equilateral configuration case in order that the LUMO falls in energy below the total internal Coulomb barriers of the molecule generated by the nuclei, V_c and the electrostatic field E_0 . The distance R_c where this occurs for zero field ($E_0=0$) is a first approximation [15,17] to the true critical distance R_c as it neglects charge-resonance effects [4–6].

The perpendicular polarization (z axis), ionization rate, curve (b), exhibits a maximum at $R_c=6.5 \text{ a.u.}$, a somewhat smaller distance. For all three cases one has the maximum ionization rates Γ (10^{13} s^{-1}): (a) 8.6; (b) 8.1; (c) 0.25 with respect to the H atom rate 0.08. Thus for equilateral H_3^{2+} , and other similar nonlinear molecules, one expects CREI to manifest itself as a strong enhancement of ionization at a critical distance $R_c \approx 5/2I_p$ as in the linear case [6]. We add

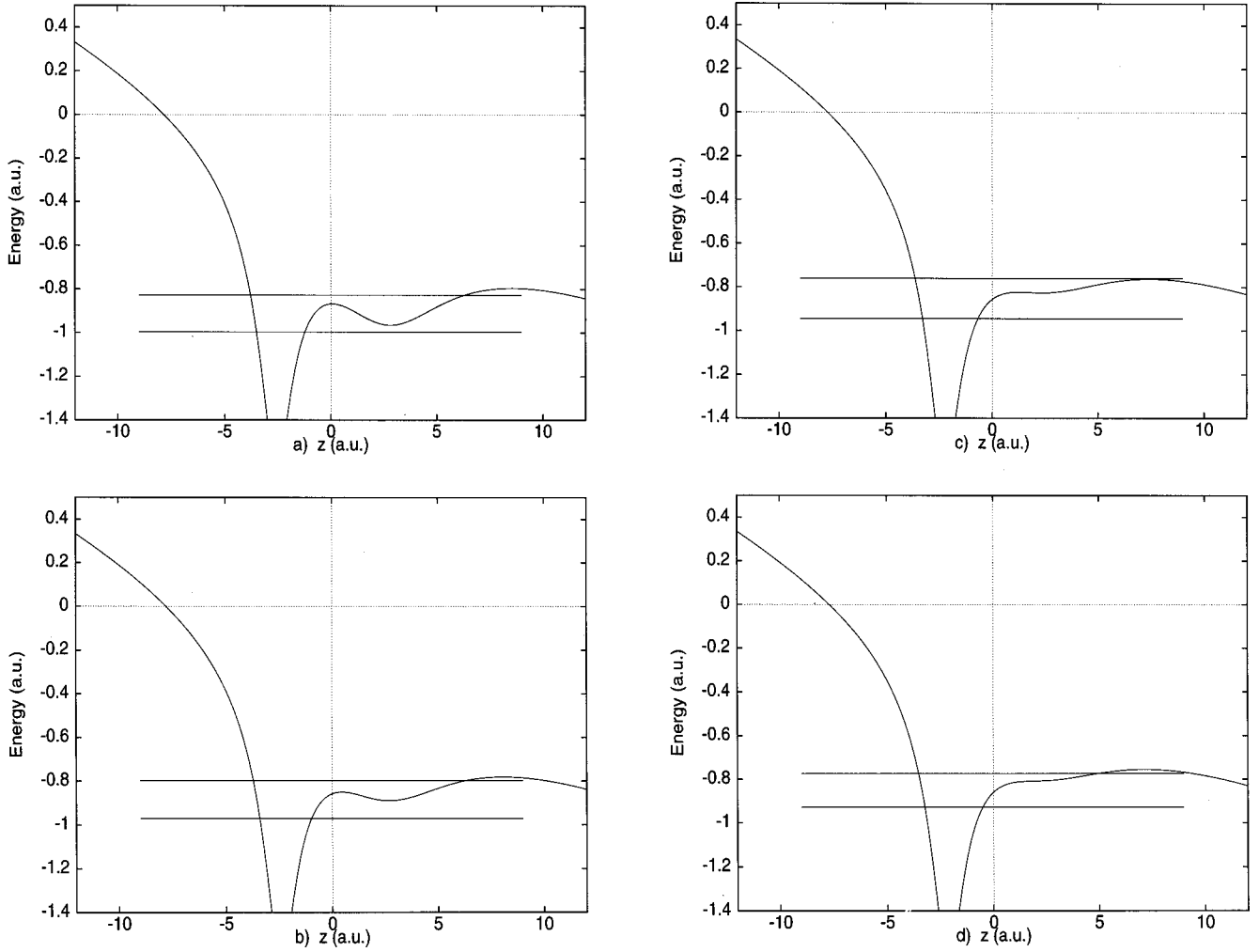


FIG. 5. HOMO-LUMO energies in a static field $E_0 = 4.8 \times 10^{-2}$ a.u. ($I_0 = 8 \times 10^{13}$ W/cm 2) at critical $R_c = 6.5$ a.u. for z polarization [Fig. 4(b)] for internal angles ϕ : (a) $\phi = 65^\circ$; (b) $\phi = 75^\circ$; (c) $\phi = 87.5^\circ$; (d) $\phi = 95^\circ$.

finally that for the equilateral case, R_c is independent of laser polarization as confirmed by Fig. 3.

Finally in Fig. 4 we present the ionization for H_3^{2+} as a function of internal angle ϕ at the two R_c 's illustrated in Fig. 3; 7 a.u. for x polarization and 6.5 a.u. for z polarization. Thus for the first case, Fig. 4(a) with the field parallel to one of the bonds which becomes parallel to the linear molecule as the angle ϕ increases to 180° , the ionization rate increases sharply between 80° and 100° , but only by about a factor of 2. The sensitivity of the ionization rate to the internal angle ϕ is much greater for the perpendicular polarization. Thus, as shown in Fig. 4(b), the rate increases by about one order of magnitude between $\phi = 70^\circ$ and 90° with a maximum around $\phi_0 = 87^\circ$.

An interpretation of intense field ionization can be made in terms of a field-induced tunneling model in the long-wavelength regime [17,21]. A criterion for the validity of such an approach is the Keldysh parameter (in a.u.)

$$\gamma = (I_p/2U_p)^{1/2} = \omega(2I_p)^{1/2}/E_0, \quad (5)$$

where I_p is the ionization potential, U_p the ponderomotive energy (see Sec. II) for a field strength E_0 . The tunneling regime is therefore defined by $\gamma < 1$ where field effects (U_p) are larger than internal Coulomb potentials (I_p). For linear

H_3^{2+} , a good estimate for I_p is $I_p = 0.5 + 2/R$ at large R where 0.5 is the I_p for H . Thus one obtains $I_p(H_3^{2+}, R = 7) \approx 0.8$ a.u. Since $U_p(I = 8 \times 10^{13}$ W/cm 2 , $\lambda = 1064$ nm) = 0.39 a.u., one obtains from Eq. (4) $\gamma \approx 1$. Clearly, under the present simulation conditions one is at the limit of the static tunneling ionization model, whereas for $\gamma > 1$ one expects a multiphoton transition description to be more adequate. We show next that the static model does allow for a correlation and an interpretation of the CREI critical angle ϕ_c observed in Fig. 4.

We illustrate the correlation between CREI and the internal angle ϕ and the positions of the field-induced HOMO and LUMO with respect to the net internal (field plus Coulomb) potential barriers in Fig. 5. The energy levels illustrated in Fig. 5 were calculated from a time-dependent propagation of the TDSE for H_3^{2+} in a static field $E_0 = 4.8 \times 10^{-2}$ a.u. ($I_0 = cE_0^2/8\pi = 8 \times 10^{13}$ W/cm 2) (see Ref. [4] for details). One observes from Fig. 5 that as the internal angle ϕ opens from the minimum equilateral angle 60° towards the maximum angle linear configuration $\phi = 180^\circ$, the upper level (LUMO in zero field) rises above the internal barrier between the protons in the bond perpendicular to the field E_0 , but then becomes retrapped for angles of $> 87^\circ$. A subtle interplay between energy separation and radiative cou-

pling which populates the upper level is responsible for the ionization maximum. Figure 5 shows that a strong correlation exists between the ionization maximum window for angles $70^\circ < \phi < 90^\circ$, Fig. 4, and the position of the upper field-induced molecular energy level with respect to the internal barrier in nonlinear H_3^{2+} , illustrated in Fig. 5. We conclude that this static field image is also useful to describe CREI in nonlinear molecules as it is for linear molecules [4,6,17]. Hence, in nonlinear molecules CREI occurs at critical distances R_c , Fig. 3, but also at critical angles ϕ_c , Fig. 4, and therefore is a universal ionization enhancement induced by short intense laser pulses. Recent Coulomb explosion measurement in linear [29] and nonlinear molecules [30] shows both CREI at large internuclear distances but also at strong nonlinear structural transitions. However, a critical angle has not yet been identified.

IV. ORIENTATIONAL EFFECTS ON IONIZATION

The ionization rates reported in Figs. 3 and 4 and discussed in the preceding section were calculated for parallel field-molecule orientations in the linear case. However intense fields via their nonlinear interaction with polarizabilities of molecules will induce alignment in the nonresonant case [11–14,31]. Resonant excitation in the nonlinear high intensity regime can also lead to laser control of molecular orientations and photodissociation angular distributions [32,33]. Recent measurements of dissociation dynamics of nonlinear molecules in intense laser fields show remarkable directional specificities with respect to the polarization of the incident field [34]. Measurements of angular distributions of ionic fragments of diatomics in intense laser fields show clear dynamic and geometric laser-induced alignment of molecules [35]. We will therefore next address orientational effects in ionization.

Our previous calculations of ionization rates in the molecules H_2^+ , H_2 , and H_3^+ based on finite element methods [36] showed that parallel (Γ_{\parallel}) ionization rates exceeded perpendicular (Γ_{\perp}) rates at equilibrium distances by about a factor of 2 to 3 for the ions whereas for neutrals H_2 this ratio was about a factor of 2 at the higher intensity, 10^{15} W/cm². In the case of equilateral H_3^+ at equilibrium ($R_e = 1.65$ a.u.), this ratio was about 1.5 whereas we have already shown in Fig. 4, that at the critical configurations $R_c = 7$ a.u. and $\phi_c = 87^\circ$, this ratio can vary by about one order of magnitude. Static field quasienergy calculations on H_2^+ also reach the conclusion that ionization rates are, in general, very sensitive to orientation, [37]. Since Coulomb explosions occur at or near the critical distances R_c for pulses sufficiently long to allow molecules to dilate to such distances, a critical assessment of angle-dependent ionization rates and alignment torques is essential near these critical distances.

We have therefore obtained ionization rates for linear H_2^+ and H_3^{2+} as a function of angle θ between the laser polarization and the molecular axis following the numerical procedure detailed in Sec. II. Ionization rates for the above laser parameters are reported in Table I for H_2^+ and Table II for H_3^{2+} as a function of angle θ and interproton distances $R = 3, 7, 9.5$ a.u. for H_2^+ and $R = 1.65$ and 6 a.u. for H_3^{2+} . Both tables illustrate the previous remark that ionization rates are always most sensitive around the critical distance R_c . Thus

TABLE I. Ionization rates Γ (10^{13} s⁻¹) for 2D-H_2^+ as a function of interproton distance R and laser orientation θ at $I = 8 \times 10^{13}$ W/cm², $\lambda = 1064$ nm laser parameters.

| θ (deg) | $R = 3$ a.u. | $R = 7$ a.u. | $R = 9.5$ a.u. |
|----------------|--------------|--------------|----------------|
| 0 | 0.0068 8 | 4.8 | 2.3 |
| 10 | 0.0083 8 | 4.7 | 2.2 |
| 20 | 0.0093 5 | 3.5 | 2.1 |
| 30 | 0.0078 0 | 2.3 | 1.7 |
| 40 | 0.0068 3 | 1.2 | 1.3 |
| 45 | 0.0070 2 | 0.76 | 1.0 |
| 50 | 0.0072 5 | 0.49 | 1.0 |
| 60 | 0.0098 1 | 0.19 | 0.78 |
| 70 | 0.0099 0 | 0.14 | 0.38 |
| 80 | 0.0099 8 | 0.14 | 0.23 |
| 90 | 0.012 2 | 0.10 | 0.20 |

for H_2^+ , $\Gamma_{\parallel}/\Gamma_{\perp} \sim 40$ at $R = 7$ a.u., 10 at $R = 9.5$ a.u. in agreement with previous 3D calculations [36]. For H_3^{2+} these ratios are ~ 2 at $R = 1.65$ a.u., ~ 100 at $R = 6$ a.u.

The above results demonstrate the importance of the critical distance R_c in intense laser field nonlinear photophysics of diatomic and triatomic molecules. Ionization rates at R_c exceed equilibrium rates by at least one order of magnitude and are most sensitive to the laser polarization around these critical distances. In the next section we calculated the corresponding field-induced torques.

V. LASER-INDUCED TORQUES AND ORIENTATION

Intense laser fields are expected to induce alignment and even orientational trapping of molecules via strong nonresonant and therefore virtual field-molecule couplings from dipole moments induced in polarizable molecules. Recent interest in such alignment has led to the concept of pendular states [13] and there is now experimental observation of deflection and guiding of molecules by such field-induced dipole forces [14]. In the present work, we have shown that nonresonant field-molecule couplings through charge-resonance effects leads to CREI at critical distances R_c for linear molecules (H_2^+ , H_3^{2+}) and critical angles θ_c for non-

TABLE II. Ionization rates, Γ (10^{13} s⁻¹) for linear equidistant H_3^{2+} as a function of interproton distance R and laser orientation θ at $I = 8 \times 10^{13}$ W/cm² and $\lambda = 1064$ nm laser parameters.

| θ (deg) | $R = 1.65$ a.u. | $R = 6$ a.u. |
|----------------|-----------------|--------------|
| 0 | 0.046 | 6.0 |
| 10 | 0.045 | 0.80 |
| 20 | 0.043 | 0.040 |
| 30 | 0.050 | 0.038 |
| 40 | 0.070 | 0.075 |
| 45 | 0.069 | 0.072 |
| 50 | 0.064 | 0.070 |
| 60 | 0.046 | 0.040 |
| 70 | 0.044 | 0.025 |
| 80 | 0.044 | 0.014 |
| 90 | 0.026 | 0.006 |

linear H_3^{2+} . In the present section we will calculate the time-dependent field-induced torques experienced by the one-electron linear H_2^+ , H_3^{2+} in the CREI region and estimate the corresponding alignment times.

Limiting ourselves to planar 2D motion, an electric field will induce a dipole moment

$$\vec{d}(t) = \alpha_{\parallel} E_x(t) \hat{i} + \alpha_{\perp} E_z(t) \hat{j}, \quad (6)$$

where

$$E_x(t) = E(t) \cos \theta, \quad E_z(t) = -E(t) \sin \theta, \quad (7)$$

and $\alpha_{\parallel}(\perp)$ are the parallel (xx) and perpendicular (zz) field components of the polarizability α . The corresponding classical torque is defined as [38],

$$N_y = \mu R^2 \ddot{\theta} = d_x(t) E_z(t) - d_z(t) E_x(t) = -\frac{\alpha}{2} E^2(t) \sin 2\theta, \quad (8)$$

where μ is the molecular reduced mass, μR^2 the moment of inertia I , and $\alpha = \alpha_{\parallel} - \alpha_{\perp}$. θ is the laser-molecule angle and y is the torque direction perpendicular to the plane of the laser-molecule system.

From Eq. (8) one obtains readily the classical pendulum equation of motion for fixed internuclear distance R ,

$$\frac{d^2 \theta}{dt^2} = -\frac{E^2(t)}{2} \left(\frac{\alpha}{I} \right) \sin 2\theta. \quad (9)$$

This can be solved in the limit of large laser frequency ω , i.e., laser periods $2\pi/\omega$ shorter than the alignment time τ (see the Appendix for more general solutions). Thus setting

$$\langle E^2(t) \rangle = E_0^2 \langle \cos^2 \omega t \rangle = \frac{E_0^2}{2},$$

gives the new high-frequency equation

$$\frac{d^2 \theta}{dt^2} = -\left(\frac{E_0^2 \alpha}{4I} \right) \sin 2\theta, \quad (10)$$

where E_0 is the maximum laser amplitude. A small-angle approximation gives the harmonic equation

$$\frac{d^2 \theta}{dt^2} + \left(\frac{E_0^2 \alpha}{2I} \right) \theta = 0, \quad (11)$$

from which one obtains the pendular frequency

$$\omega_p = (E_0^2 \alpha / 2I)^{1/2}. \quad (12)$$

Equation (9) can be solved for the more general case in terms of elliptic integrals K , allowing to define the alignment time for motion from some initial angle θ_0 to a final $\theta = 0$, [38],

$$\tau = \frac{1}{\omega_p} K(\sin \theta_0), \quad (13)$$

where ω_p is the field-induced pendular frequency defined in Eq. (12) and K is an elliptic integral [39]. For very small

angle θ_0 , $K(0) = \pi/2$ so that $\tau_p = \pi/(2\omega_p)$ corresponds to one-fourth of a pendular period.

Our previous calculations of α for H_2^+ at 1064 nm [36] allow us to estimate ω_p and τ at intensity 10^{14} W/cm², where $E_0 = 5.3 \times 10^{-2}$ a.u. Thus with $\alpha = 3.3$ a.u., $I = 1800$ a.u. ($R = 1.4$ a.u.) one obtains readily $1/\omega_p = 625$ a.u. = 15 fs, which gives a pendular period $2\pi/\omega_p = 94$ fs. The corresponding alignment time (one-fourth of cycle) $\tau_p = 23$ fs. This is the small-angle oscillation limit. Using values of elliptic integrals, Eq. (13) gives $\tau = 80$ fs for alignment from $\theta_0 = 89^\circ$ and $\tau = 30$ fs for $\theta_0 = \pi/4$. Thus at intensity 10^{14} W/cm², one estimates that the alignment time for H_2^+ at $R = 1.4$ a.u. from the above classical model should be $80 \text{ fs} > \tau > 30 \text{ fs}$. The result is frequency independent as we have used a high-frequency approximation (see the Appendix for the general solution where it is shown that τ is indeed nearly frequency independent).

Knowing that preferential ionization occurs at $R_c \approx 7$ a.u. for H_2^+ , Eqs. (12) and (13) predict that the alignment time is proportional to $(I/\alpha)^{1/2} E_0 = (\mu/\alpha)^{1/2} R/E_0$. The polarizability α is expected to vary as the internuclear distance R due to the charge-resonance interaction responsible for CREI. Adopting the simple model that α is proportional to the volume of the molecule, $\alpha \sim R^3$ [40] one obtains the simple rule that $\tau \propto E_0^{-1} (\mu/R)^{1/2}$. Thus one predicts that alignment times should decrease linearly with the field strength E_0 , decrease as $R^{-1/2}$, and increase with the reduced mass as $\mu^{1/2}$. The above considerations have assumed that the first-order polarizability α is adequate to describe the field-molecule interaction and that there is no ionization. We examine below by accurate solutions of the TDSE for 2D H_2^+ and H_3^{2+} the actual torques produced by an intense laser field.

We illustrate in Fig. 6 the calculated laser-induced dipoles $d_x(t)$, $d_z(t)$ obtained from Eq. (4) for H_2^+ at $R = 9.5$ a.u., $I = 10^{14}$ W/cm², $\lambda = 1064$ nm, and laser angle $\theta = 45^\circ$. The corresponding torque $N_y(t)$ calculated from Eq. (8) is illustrated in Fig. 7. Figure 6 shows that after the five cycle pulse rise the induced dipoles follow the field according to the perturbative expression (6). The small asymmetry on the $d_x(t)$ component which is due to the pulse rise, Fig. 6, results in the torque, Fig. 7, not following the perturbative expression (8) exactly. Thus Fig. 7 illustrates two sets of maxima with unequal amplitudes whereas Eq. (8) predicts equal amplitudes repeating at half-cycles. Finally in Fig. 8 we present the torques $N_y(t)$ for the two different laser-molecule orientations: (a) $\theta = 30^\circ$ and (b) $\theta = 60^\circ$. Since from Eq. (8), $N_y(t) \propto \sin 2\theta$ and $\sin(\pi - 2\theta) = \sin(2\theta)$, one would expect the torque to be the same for these two angles, i.e., $\theta = 30^\circ$ and 60° . Figure 8 shows clearly this is not the case. The torques have opposite sign and exhibit different time-dependent periodicities. Thus Fig. 8(a) ($\theta = 30^\circ$) is similar to Fig. 7 ($\theta = 45^\circ$). This is consistent with the fact that in these two cases the $d_x(t)$ component is dominant. Figure 8(b) corresponds to a torque where $d_z(t)$ is dominant as can be verified from Table III. Table I shows further that the ionization rates at 30° exceeds that at 60° by a factor of 2. Thus the response of the molecule at these two orientations is quite different in the ionization regime. This results in different ionization rates and also different torques, contrary to the perturbative regime defined by Eq. (8).

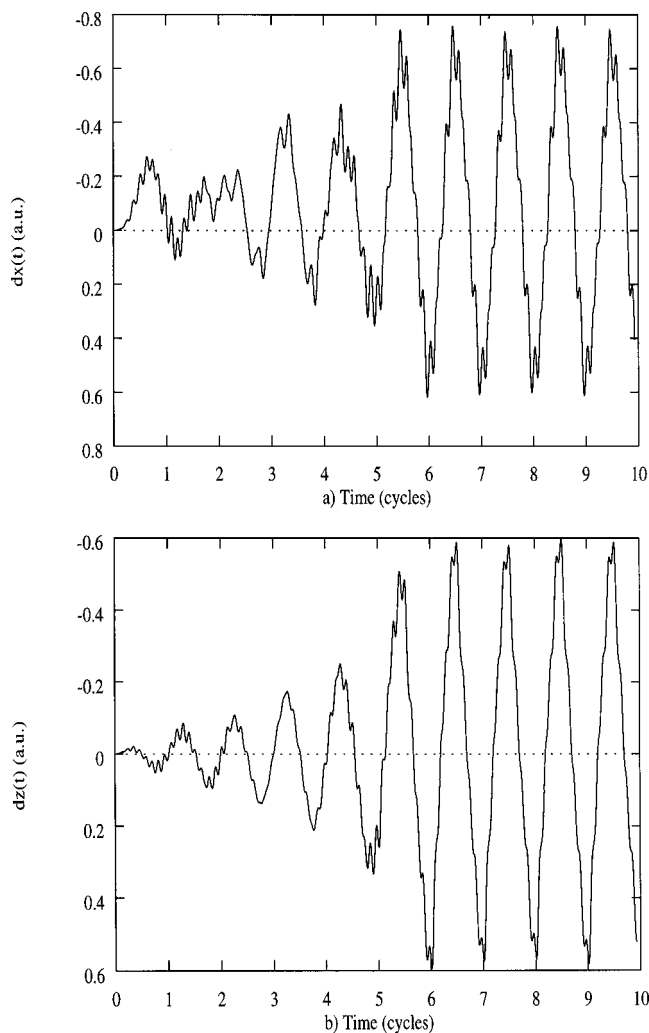


FIG. 6. Laser-induced dipoles for H_2^+ at $R=9.5$ a.u., $I=1064$ W/cm 2 , $\lambda=10^{14}$ nm, and laser angle $\theta=45^\circ$: (a) $d_x(t)$; (b) $d_z(t)$.

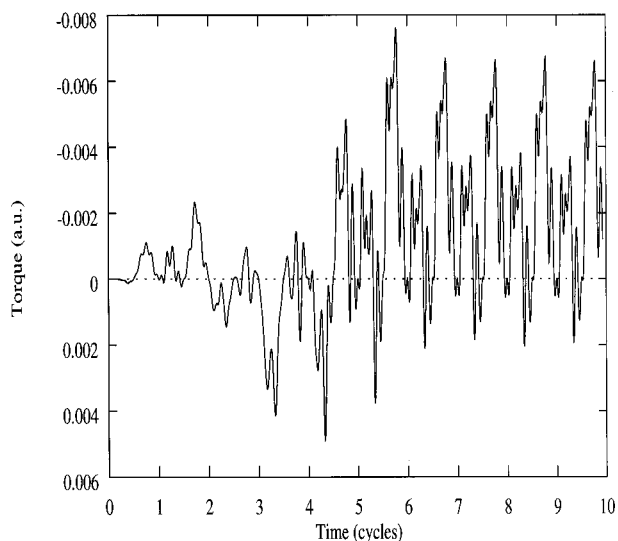


FIG. 7. Laser-induced torque $N_y(t)$, Eq. (8) for H_2^+ at $R=9.5$ a.u., $I=10^{14}$ W/cm 2 , $\lambda=1064$ nm, and laser orientation $\theta=45^\circ$, corresponding to dipoles, Fig. 6.

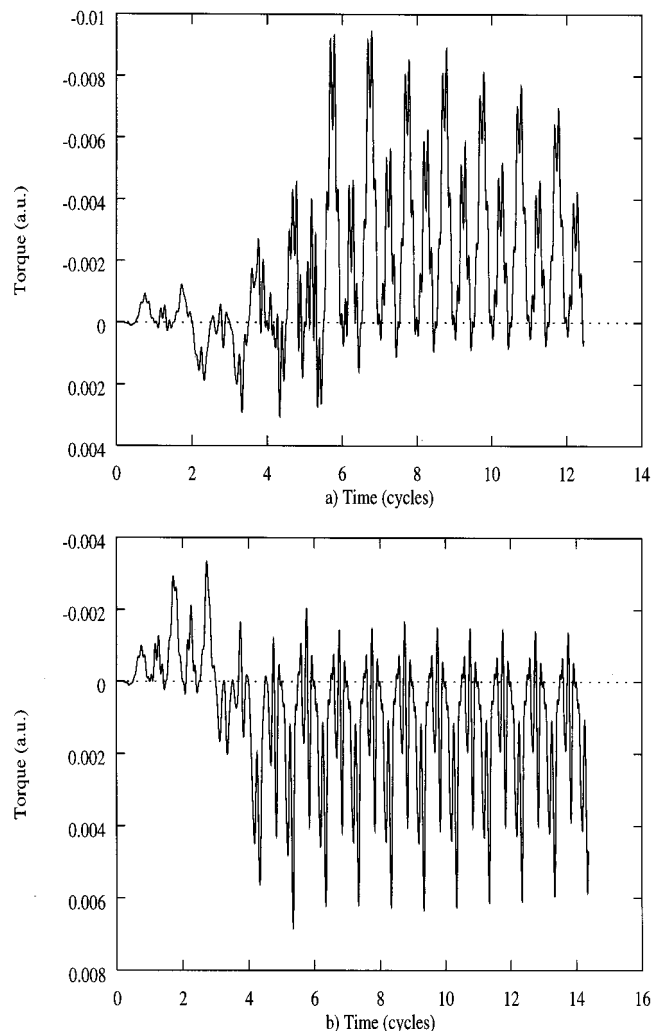


FIG. 8. Laser-induced torques $N_y(t)$, Eq. (8), for H_2^+ at $R=9.5$ a.u., $I=10^{14}$ W/cm 2 , $\lambda=1064$ nm, for laser orientation: (a) $\theta=30^\circ$; (b) $\theta=60^\circ$.

Comparisons of ionization rates for H_2^+ , Table I and H_3^{2+} , Table II and Figs. 3 and 4 show that these are most sensitive to laser orientation θ at the CREI distances, $R_c=7$ and 6 a.u. The comparisons of the dipoles and torques, Table III and IV, show the same effect, largest variations of these physical parameters occur at R_c as a function of the laser angle θ , and these do not conform to the perturbative expressions (6)–(8). In the discussion for H_2^+ , following Eq. (13), we estimated the alignment time (at $I=10^{14}$ W/cm 2 , $\lambda=1064$ nm) to be $80\text{ fs} > \tau > 30\text{ fs}$ for $R=1.4$ a.u. At the critical distance R_c , 7 a.u., since τ scales as $(I/\alpha)^{1/2} \sim R^{-1/2}$, shorter alignment times should be in order. Perusal of Table III for H_2^+ shows torques are maximum at $R_c=7$, thus implying shorter τ 's. However, such torques exhibit an unusual property at R_c , they change signs at $\theta=35^\circ$ and 65° , i.e., zero torque occurs at these angles, implying ‘‘trapping’’ of the molecular ion at such angles. From the ionization rates in Table I one estimates the lifetimes of these angular states to be 60 fs (35°) and 600 fs (65°).

H_3^{2+} is more amenable to an analytical analysis following Tables II and IV. Thus at the equilibrium distance of linear H_3^+ [36], $R=1.65$ a.u., the torque N_y , Table IV ($I=$

TABLE III. Maximum dipoles $d_{x(z)}$ and torques N_y for 2D- H_2^+ at $\lambda = 1064$ nm, $I = 10^{14}$ W/cm² laser parameters as a function of laser orientation θ .

| θ (deg) | $R=3$ | | | $R=7$ | | | $R=9.5$ | | |
|-------------------|----------------|----------------|---------|----------------|----------------|--------|----------------|----------------|--------|
| | dx (a.u.) | dz (a.u.) | N_y | dx (a.u.) | dz (a.u.) | N_y | dx (a.u.) | dz (a.u.) | N_y |
| 0 | 0.80 | 0 | 0 | 3.8 | 0 | 0 | 1.5 | 0 | 0 |
| 10 | 0.78 | 0.03 | -0.030 | 3.0 | 0.3 | 0.004 | 1.5 | 0.3 | 0.0035 |
| 20 | 0.75 | 0.06 | -0.020 | 1.8 | 0.5 | 0.012 | 1.4 | 0.5 | 0.006 |
| 30 | 0.70 | 0.10 | -0.0006 | 1.0 | 0.6 | 0.013 | 1.1 | 0.6 | 0.008 |
| 40 | 0.61 | 0.13 | 0.0007 | 1.5 | 0.5 | -0.020 | 0.95 | 0.6 | 0.0075 |
| 45 | 0.60 | 0.15 | 0.0011 | 1.5 | 0.5 | -0.025 | 0.77 | 0.6 | 0.006 |
| 50 | 0.57 | 0.17 | 0.0021 | 1.5 | 0.4 | -0.029 | 0.57 | 0.42 | 0.0045 |
| 60 | 0.41 | 0.18 | 0.0036 | 1.0 | 0.3 | -0.020 | 0.4 | 0.3 | -0.006 |
| 70 | 0.29 | 0.19 | 0.0048 | 0.9 | 0.3 | 0.04 | 0.3 | 0.23 | 0.004 |
| 80 | 0.14 | 0.21 | 0.0059 | 1.1 | 0.4 | 0.045 | 0.3 | 0.2 | 0.008 |
| 90 | 0 | 0.21 | 0 | 0 | 0.4 | 0 | 0 | 0.3 | 0 |

8×10^{13} W/cm²), follows the $\sin 2\theta$ law, Eq. (18). This allows us to evaluate the parameter $(\alpha E_0^2)/2 = N_y(45^\circ) = 0.006$ a.u. The alignment time τ is obtained from Eq. (13) as $\pi/(2\omega_p) = \pi/2(I/N)^{1/2} = 49$ fs, where $l = 2m_H R^2 = 9800$ a.u. The maximum ionization rate occurs at $\theta = 45^\circ$, $\Gamma = 0.07 \times 10^{13}$ s⁻¹, with a corresponding lifetime of 1.4 ps, giving the molecular ion ample time to align at $R = 1.65$ a.u. before complete ionization. At the critical distance $R_c = 6$ a.u. (Table IV), the torque N_y grows steadily with orientation angle θ . Taking $N_y(45^\circ) = 0.05$ as an approximation to $\alpha E_0^2/2$ again, and using $l = 1.3 \times 10^5$ a.u., gives $\tau = 62$ fs for the alignment time of H_3^{2+} at $R_c = 6$ a.u., $I = 8 \times 10^{13}$ W/cm². The corresponding ionization rates vary rapidly (Table II) with one maximum of 0.07×10^{13} s⁻¹ at $\theta = 45^\circ$, corresponding to a lifetime also of 1.4 ps. Clearly at $R_c = 6$ a.u., the ion has again sufficient time to align to $\theta = 0^\circ$ where it will rapidly undergo CREI with a lifetime of 16 fs.

VI. CONCLUSION

We have performed exact fixed nuclei (Born-Oppenheimer) calculations of ionization rates and torques for

the one-electron systems, 2D- H_3^+ and H_3^{2+} as a function of internuclear distance R , internal angle ϕ for H_3^{2+} , and laser orientation θ . Ionization maxima, exceeding that of the H atom were found to occur at critical distance R_c for both systems and also at critical internal angles ϕ_c for H_3^{2+} . These maxima were attributed to CREI and were shown to be the result of laser-induced displacements of the LUMO via charge-resonance effects above the field-induced static Coulomb barriers.

Laser orientation-dependent-induced dipole moments and torques were also obtained from the numerical solutions. As in the case of ionization rates, these were found to be the largest and the most sensitive to orientation around the critical CREI configurations. It was found that for intensities around 10^{14} W/cm², torques are sufficiently large at equilibria and at critical CREI configurations to allow for orientation before the onset of complete ionization. The present numerical results also indicate that at the CREI critical distances, torques can change sign due to the highly nonlinear, nonperturbative nature of the molecule-field interactions. This implies that vanishing torques will occur at particular angles, leading hence to orientational trapping at these angles

TABLE IV. Maximum dipoles $d_{x(z)}$ and torques N_y for 2D linear H_3^{2+} at $\lambda = 1064$ nm, $I = 8 \times 10^{13}$ W/cm² laser parameters as a function of laser orientation θ .

| θ (deg) | $R=6$ | | | $R=1.65$ | | |
|-------------------|----------------|----------------|-------|----------------|----------------|--------|
| | dx (a.u.) | dz (a.u.) | N_y | dx (a.u.) | dz (a.u.) | N_y |
| 0 | 2.2 | 0 | 0 | 0.30 | 0 | 0 |
| 10 | 2.0 | 0.1 | 0.005 | 0.20 | 0.03 | 0.0020 |
| 20 | 1.9 | 0.14 | 0.010 | 0.25 | 0.05 | 0.0030 |
| 30 | 1.8 | 0.2 | 0.012 | 0.28 | 0.11 | 0.0045 |
| 40 | 2.6 | 1.0 | 0.050 | 0.23 | 0.15 | 0.0055 |
| 50 | 2.5 | 2.0 | 0.025 | 0.20 | 0.17 | 0.0060 |
| 60 | 2.0 | 1.0 | 0.035 | 0.15 | 0.15 | 0.0043 |
| 70 | 2.0 | 0.7 | 0.050 | 0.10 | 0.15 | 0.003 |
| 80 | 1.9 | 0.4 | 0.060 | 0.05 | 0.17 | 0.0020 |
| 90 | 0 | 0.15 | 0 | 0 | 0.18 | 0 |

at intensities above 10^{14} W/cm².

APPENDIX

The pendulum equation (9) can be rewritten as a function of the generalized field area

$$\sigma(t) = \int E(t) dt, \quad (\text{A1})$$

$$\frac{d^2 \theta}{d\sigma^2(t)} = \gamma \sin 2\theta, \quad (\text{A2})$$

where $\gamma = \alpha/(2l)$, the ratio of polarizability to moment of inertia. For small angles $\sin \theta \approx \theta$, we obtain a harmonic equation

$$\frac{d^2 \theta}{d\sigma^2} + \omega_\theta^2 \theta = 0, \quad \omega_\theta = (\alpha/l)^{1/2}, \quad (\text{A3})$$

$$\theta(t) = \theta_0 \cos[\omega_\theta \sigma(t)]. \quad (\text{A4})$$

For a constant pulse shape E_0 , $E(t) = E_0 \cos \omega t$, $\sigma(t) = (E_0/\omega) \sin \omega t$, one obtains

$$\begin{aligned} \theta(t) &= \theta_0 \cos\left(\frac{\omega_\theta E_0}{\omega} \sin \omega t\right), \\ \theta(t) &= \theta_0 \left[J_0\left(\frac{\omega_\theta E_0}{\omega}\right) \right. \\ &\quad \left. + 2 \sum_{k=1}^{\infty} J_{2k}\left(\frac{\omega_\theta E_0}{\omega}\right) \cos(k\omega t) \right]. \end{aligned} \quad (\text{A5})$$

In the high-frequency limit $\omega_\theta/\omega \ll 1$, one obtains from asymptotic expressions of the integer Bessel function J_n [39],

$$\theta(t) \propto \theta_0 J_0\left(\frac{\omega_\theta E_0}{\omega}\right) \approx \theta_0 \left[1 - \frac{\omega_\theta^2 E_0^2}{\omega^2} + \dots \right] \approx \theta_0 [1 - \omega_p^2/2\omega^2], \quad (\text{A6})$$

where ω_p is the field-induced pendular frequency, Eq. (12). Equation (6) predicts, therefore, an average shift of the initial angle θ_0 by the fraction $\omega_p^2/2\omega^2$.

The most general solution of Eq. (2) for alignment from θ_0 to $\theta=0$ is [38]

$$\sigma(\tau) = \gamma^{-1/2} K(\sin \theta_0), \quad (\text{A7})$$

where K is an elliptic integral [39].

For a constant periodic field $E(t) = E_0 \cos \omega t$, one obtains the transcendental equation for the alignment time τ .

$$\sin(\omega \tau) = \frac{\omega}{\sqrt{2}\omega_p} K(\sin \theta_0), \quad (\text{A8})$$

as compared to the *high-frequency* limit, Eq. (13). For small θ_0 , $K(0) = \pi/2$, and assuming $\sin \omega t \approx \omega t$, one obtains

$$\tau = \frac{1}{\sqrt{2}} \frac{\pi}{2\omega_p}, \quad (\text{A9})$$

as compared to the high-frequency limit $\tau = \pi/2\omega_p$ from Eq. (13).

Another limit, the *low-frequency* or near static field limit can be now obtained from the more general solution (8) by setting again $\sin \omega t \approx \omega t$,

$$\tau = \frac{K(\sin \theta_0)}{\sqrt{2}\omega_p}. \quad (\text{A10})$$

This differs from the high-frequency limit equation (13) by the same factor $1/\sqrt{2}$ as the small-angle equation (9),

We conclude from the more general frequency-dependent transcendental equation (8) for the alignment time τ that the low-frequency t , Eq. (10) and the high-frequency τ , Eq. (13), are nearly the same, so that the alignment time can be considered to be frequency independent.

-
- [1] M. Gavrilu, *Atoms in Laser Fields* (Academic, New York, 1992).
- [2] A. D. Bandrauk, *Molecules in Laser Fields* (Dekker, New York, 1994), Chaps. 3–5.
- [3] T. Zuo, S. Chelkowski, and A. D. Bandrauk, Phys. Rev. A **48**, 3837 (1993).
- [4] T. Zuo and A. D. Bandrauk, Phys. Rev. A **52**, 2511 (1995).
- [5] S. Chelkowski and A. D. Bandrauk, J. Phys. B **28**, L723 (1995).
- [6] H. Yu, T. Zuo, and A. D. Bandrauk, Phys. Rev. A **54**, 3290 (1996); J. Phys. B **31**, 1533 (1998).
- [7] M. Schmidt, D. Normand, and C. Cornaggia, Phys. Rev. A **50**, 5037 (1994).
- [8] E. Constant, H. Stapelfeldt, and P. B. Corkum, Phys. Rev. Lett. **76**, 4140 (1996).
- [9] G. N. Gibson, M. Li, C. Guo, and J. Neva, Phys. Rev. Lett. **79**, 202 (1997).
- [10] D. Normand, L. A. Lompré, and C. Cornaggia, J. Phys. B **25**, L497 (1992).
- [11] P. Dietrich, D. Strickland, M. Laberge, and P. B. Corkum, Phys. Rev. A **47**, 2305 (1993).
- [12] C. Cornaggia, M. Schmidt, and D. Normand, Phys. Rev. A **51**, 1431 (1995).
- [13] B. Friedrich and D. Hershbach, Phys. Rev. Lett. **74**, 4623 (1995).
- [14] H. Stapelfeldt, H. Sakai, E. Constant, and P. B. Corkum, Phys. Rev. Lett. **79**, 2787 (1997); Phys. Rev. A **55**, 3319 (1997); **57**, 2794 (1998).
- [15] K. Codling, L. Frasiniski, and P. Hatherly, J. Phys. B **22**, L321 (1989); **26**, 783 (1993).

- [16] R. S. Mulliken, *J. Chem. Phys.* **7**, 20 (1939).
- [17] T. Seiderman, M. Ivanov, and P. B. Corkum, *Phys. Rev. Lett.* **75**, 2819 (1995).
- [18] S. Chelkowski, A. Conjusteau, T. Zuo, and A. D. Bandrauk, *Phys. Rev. A* **54**, 3235 (1996).
- [19] S. Chelkowski, C. Foisy, and A. D. Bandrauk, *Phys. Rev. A* **57**, 1176 (1998).
- [20] M. J. DeWitt and R. J. Levis, *J. Chem. Phys.* **102**, 8670 (1995).
- [21] M. J. DeWitt and R. J. Levis, *Chem. Phys.* **218**, 211 (1997); *J. Chem. Phys.* **108**, 7045 (1998).
- [22] J. U. Brackhill and B. I. Cohen, *Multiple Time Scales* (Academic, Orlando, 1985).
- [23] D. M. Villeneuve, M. Y. Ivanov, and P. B. Corkum, *Phys. Rev. A* **54**, 736 (1996).
- [24] A. D. Bandrauk, S. Chelkowski, and E. Constant, *Phys. Rev. A* **56**, 2537 (1997).
- [25] M. D. Feit, J. A. Fleck, and A. Steiger, *Chem. Phys. Lett.* **47**, 412 (1982).
- [26] A. D. Bandrauk and H. Shen, *J. Chem. Phys.* **99**, 1185 (1993).
- [27] G. C. Schatz and M. A. Ratner, *Quantum Mechanics in Chemistry* (Prentice-Hall, Englewood Cliffs, NJ, 1993), Chap. 7.
- [28] J. K. Burdett, *Chemical Bonding in Solids* (Oxford University Press, New York, 1995), Chap. 8.
- [29] C. Cornaggia, *Phys. Rev. A* **54**, 2555 (1996); **57**, 4572 (1998).
- [30] D. Mathur, V. R. Bhardwaj, G. R. Kumar, F. Rajgara, and C. Safvan, *Phys. Scr.* **T73**, 254 (1997).
- [31] B. Friedrich and D. Herschbach, *J. Phys. C* **99**, 15 686 (1995).
- [32] A. D. Bandrauk and J. F. McCann, *Phys. Rev. A* **42**, 2806 (1990); *J. Chem. Phys.* **96**, 903 (1992).
- [33] E. Aubanel and A. D. Bandrauk, *Chem. Phys. Lett.* **229**, 169 (1994); *Chem. Phys.* **198**, 159 (1995).
- [34] G. R. Kumar, P. Gross, C. Safvan, F. Rajgara, and D. Mathur, *J. Phys. B* **29**, L481 (1996); *Phys. Rev. A* **53**, 3098 (1996).
- [35] J. H. Posthumus, M. K. Thomas, K. Codling, and L. J. Frain-ski, *J. Phys. L* (to be published).
- [36] H. Yu and A. D. Bandrauk, *J. Chem. Phys.* **102**, 1257 (1995).
- [37] M. Plumer and J. F. McCann, *J. Phys. B* **30**, L401 (1997).
- [38] L. Landau and L. Lifschitz, *Mechanics* (Addison-Wesley/Pergamon, New York, 1960), Chap. 3.
- [39] D. Zwillinger, *Standard Mathematical Tables*, 30th ed. (CRC, New York, 1996).
- [40] D. W. Davies, *Theory of Electric and Magnetic Properties of Molecules* (Wiley, New York, 1967).